Journal of Instrumentation

SISSA

PAPER • OPEN ACCESS

Highlights of recent SPIDER results and improvements

To cite this article: E. Sartori *et al* 2023 *JINST* **18** C09001

View the article online for updates and enhancements.

You may also like

- Development of Self-Discharge Point Visualization Technique inside Lithium-Ion Battery
Takao Mizutani, Kenjiro Kimura, Noriaki Kimura et al.
- The activities and funding of IRPA: an overview
Geoffrey Webb
- Invited: The Impact of a (Si)Ge Heterojunction on the Analog Performance of Vertical Tunnel FETs
Paula Ghedini Der Agopian, J. A. Martino, Anne Vandooren et al.

This content was downloaded from IP address 149.132.187.54 on 27/03/2024 at 13:35

Jinst

Published by IOP Publishing for Sissa Medialab

Received: *January 31, 2023*
Accepted: *July 7, 2023*
Published: *September 4, 2023*

8th International Symposium on Negative Ions, Beams and Sources
Orto Botanico, Padova, Italy
2–7 October 2022

Highlights of recent SPIDER results and improvements

E. Sartori,[a,b,*] R. Agnello,[a,c] M. Agostini,[a] M. Barbisan,[a] M. Bigi,[a] M. Boldrin,[a] M. Brombin,[a] V. Candeloro,[a,b] R. Casagrande,[a] S. Dal Bello,[a] M. Dan,[a] B. Pouradier Duteil,[a,c] M. Fadone,[a] L. Grando,[a] P. Jain,[a] A. Maistrello,[a] I. Mario,[a,h] R. Pasqualotto,[a] M. Pavei,[a] A. Pimazzoni,[a] C. Poggi,[a] A. Rizzolo,[a] A. Shepherd,[a,d] M. Ugoletti,[a] P. Veltri,[e] B. Zaniol,[a] P. Agostinetti,[a] D. Aprile,[a] G. Berton,[a] C. Cavallini,[a] M. Cavenago,[f] G. Chitarin,[a,b] G. Croci,[g] R. Delogu,[a] M. De Muri,[a] M. De Nardi,[a,b] S. Denizeau,[a] F. Fellin,[a] A. Ferro,[a] E. Gaio,[a] C. Gasparrini,[a] A. Luchetta,[a] F. Lunardon,[a,b] G. Manduchi,[a] N. Marconato,[a,b] D. Marcuzzi,[a] O. McCormack,[a,h] R. Milazzo,[a] A. Muraro,[g] T. Patton,[a] N. Pilan,[a] M. Recchia,[a] A. Rigoni-Garola,[a] F. Santoro,[a,b] B. Segalini,[a,b] M. Siragusa,[a] M. Spolaore,[a] C. Taliercio,[a] V. Toigo,[a] P. Zaccaria,[a] R. Zagorski,[a,g] L. Zanotto,[a] M. Zaupa,[a] M. Zuin[a] and G. Serianni[a]

[a] *Consorzio RFX, CNR, ENEA, INFN, University of Padova, Acciaierie Venete SpA, Corso Stati Uniti 4, 35127 Padova, Italy*
[b] *Università degli Studi di Padova, via VIII Febbraio 2, 35122 Padova, Italy*
[c] *Ecole Polytechnique Fédérale de Lausanne (EPFL) - Swiss Plasma Center (SPC), 1015 Lausanne, Switzerland*
[d] *CCFE, Culham Science Centre, Abingdon OX14 3DB, Oxon, U.K.*
[e] *ITER Organization (IO), Route de Vinon sur Verdon, CS 90 046, F-1, 3067 St. Paul-lez-Durance, France*
[f] *Istituto Nazionale Fisica Nucleare, Laboratori Nazionali di Legnaro, Viale dell'Università, 2, 35020 Legnaro, Italy*
[g] *National Centre for Nuclear Research (NCBJ), PL-05-400 Otwock, Poland*
[h] *University of Milano-Bicocca, Piazza della Scienza 3, Milano, Italy*

E-mail: emanuele.sartori@igi.cnr.it

Abstract: Three years of experiments on SPIDER allowed characterization of the main features of the source plasma and of the negative ion beam, in the original design configuration. For the large dimensions of the source chamber, and of the extraction area, the investigation of the single-beamlet currents and of the source plasma uniformity had to be carried out to extend the knowledge gained in smaller prototype sources. The configuration of the multiple RF drivers and filter field topologies were found to cause a peculiar behavior in the plasma confinement in the

*Corresponding author.

© 2023 The Author(s). Published by IOP Publishing Ltd on behalf of Sissa Medialab. Original content from this work may be used under the terms of the Creative Commons Attribution 4.0 licence. Any further distribution of this work must maintain attribution to the author(s) and the title of the work, journal citation and DOI.

https://doi.org/10.1088/1748-0221/18/09/C09001

2023 JINST 18 C09001

drivers, creating left-right asymmetries which were also visible in the extracted negative ion currents, even after the early implementation of a new scheme of plasma-grid current send and return busbars that greatly improved performance at high filter fields. The plasma properties in the driver and expansion region as well as the positive ion energy at the extraction region were studied in different experimental conditions, and interpreted also with the support of numerical models, suggesting that an improved plasma confinement could contribute to the increase of the plasma density, and to a certain extent to a lowering of the plasma potential profile; both effects shall contribute to increase the presence of cold negative ions for the formation of low-divergence beamlets. Early results related to unwanted RF discharges on the back of the plasma source and the gas conductance of the beam source suggested the reduction of the vessel pressure as mitigation, leading to the definition of a new pumping system. The difficulties related to the simultaneous operation, stable control and high-power operation of multiple RF self-oscillating vacuum tube based RF generators were an unambiguous obstruction to the experimentation, calling for the implementation of RF solid-state amplifiers. The initial tests related to caesium management, the non-uniform plasma properties at different locations across the plasma grid, and the challenges in the measurement of the current and divergence of the accelerated beamlet, unambiguously resulted in the need of new diagnostic systems to investigate with better resolution the spatial uniformities. This contribution summarises how the main experimental findings in the previous experimental campaigns are driving modifications to the SPIDER experiment, during the present shut down, in view of future operations.

KEYWORDS: Ion sources (positive ions, negative ions, electron cyclotron resonance (ECR), electron beam (EBIS)); Plasma generation (laser-produced, RF, x ray-produced); Beam-line instrumentation (beam position and profile monitors, beam-intensity monitors, bunch length monitors); Accelerator modelling and simulations (multi-particle dynamics, single-particle dynamics)

2023 JINST 18 C09001

Contents

1 Results of the prototype source SPIDER in view of ITER neutral beams 1

2 Measurement of the beam current 2

3 Control of caesium evaporation and improvement of the emission nozzle 3

4 Vertical and horizontal homogeneity among RF drivers 4

5 Effect of magnetic fields on the plasma inside drivers 8

6 Single-beamlet optics 9

7 Expected conditions with improved pumping system 10

8 Conclusions 11

2023 JINST 18 C09001

1 Results of the prototype source SPIDER in view of ITER neutral beams

The full-size prototype source for the ITER heating neutral beam (HNB) has been in operation since 2018 at the Neutral Beam Test Facility (NBTF). The prototype source, named SPIDER, has ambitious targets [1] in terms of: the negative ion current density of each single beamlet composing the beam; the uniformity over the large extraction area, and the single-beamlet optics. SPIDER uses the RF-driven concept developed at IPP [2]; however, it is the first of its kind in terms of dimensions, and it employs the vacuum insulation concept for voltage holding (following the same ITER HNB design concept). These two aspects produced unexpected issues during the initial phases of operation [3], mainly due to the relatively high vessel pressure and the presence of breakdowns outside the source. Thanks to the application of a mask to cover most of the extraction apertures, in 2021 the extraction of high-current negative ion beamlets was demonstrated with the addition of caesium to the source plasma [4]. During this first operation with caesium, aspects worthy of improvement have been identified, aiming at possible technological improvements related to the plasma source and the negative ion beam formation. In addition to the design improvements already identified in the prototype sources at IPP, mainly concerning the use of solid-state amplifiers for powering the eight drivers of SPIDER, and to the introduction of a new pumping system with high pumping speed and capacity for hydrogenic species, the results of the source operation have been analysed to identify further design improvements, and to identify R&D topics for the source optimization in the following years. This paper proposes and discusses a few paths to improve the SPIDER beam in view of the experimental results obtained so far.

2 Measurement of the beam current

The measurement of the negative-ion beam current is not straightforward, due to stray particles and ion-induced secondary emissions. The experience with isolated beamlets, i.e. with a mask covering most apertures at the Plasma Grid (PG) [5], has been extremely useful as training in view of the full beam operation with 1280 beamlets. In general, four aspects are worth noting. First, a very good agreement was found among substantially different beam diagnostics (see figure 1), namely: electrical measurements at the intrumented beam dump combined with infra-red calorimetry to identify the single-beamlet contribution [6]; beamlet current measurement via current sensors installed immediately outside the accelerator [7, 8]; cameras of the visible beam tomography, at least in relative terms [9]. Second, the beamlet current at full acceleration estimated by these diagnostics was of the order of roughly 80% of the acceleration current measured by the high-voltage power supplies of the extraction grid and acceleration grid [10], with a possible explanation due to the many secondary charges produced by negative ions during acceleration. The rather low total beam current, with respect to the high full-range of the power supply measurement, might also play a role in giving an imprecise measurement. Third, the maximum beamlet current could be rather different and depends on the beamlet position, as well as on the source parameters; since the extraction and acceleration voltages cannot be adapted on each beamlet to match the extracted current, different single-beamlet perveances coexist and the source will always operate with a compromise condition that minimizes the average beamlet or beam divergence. Fourth, the operation with isolated beamlets allowed the emittance scanner and the beam emission spectroscopy (both measuring the ion trajectories in velocity space) to identify the broad components in the negative ion optics [11], and this effect appears to be rather pronounced even in the direction perpendicular to the deflection caused by the electron deflection magnets.

For the future operation with multiple beamlets, with axis-to-axis distances of 20 mm along the horizontal direction and 22 mm along the vertical one, none of the aforementioned diagnostics will be capable of identifying the current of each single beamlet. However, the experience gained from the recent campaigns on the method to derive the beam current from the instrumented beam dump can be used. An R&D activity for the development of customized flux-gate sensors to measure the beamlet group current (i.e. 80 adjacent beamlets) was started given the successful results obtained with single-beamlet current sensors. Unfortunately, the non-uniformities in terms of beamlet current also appear to be present within the beamlet group [12] and do not to depend on the beamlet masking [13]; the result on the scale of the beamlet group was unexpected, and the limits of either the tomographic reconstruction or the IR imaging to estimate the single-beamlet current within the beamlet group have to be tested as soon as possible to continue this assessment in future operations without PG mask. To allow optics scans as a function of the extraction voltage, the clearance at the extraction grid aperture will be increased by machining the tapering on the downstream side, to allow full transmission of beamlets even if not at perveance match. This is essential to quantify, from the accelerated beamlets, the non-uniformity of the extracted current. For the complete characterization of the beam optics in the phase space, the design and prototyping of many "beamlet plugs" was carried out to allow the isolation of a few beamlets by closing surrounding apertures of the plasma grid: with this configuration, to be applied only to a limited number of beamlets, it will be possible to continue the single-beamlet optics study via IR calorimetry and the emittance scanner [14], for the optimization

2023 JINST 18 C09001

in view of the ITER heating and diagnostic neutral beams (i.e. to calculate the transmission to the ITER plasma, but also to verify the possibility of beam halo interception by the accelerator grids).

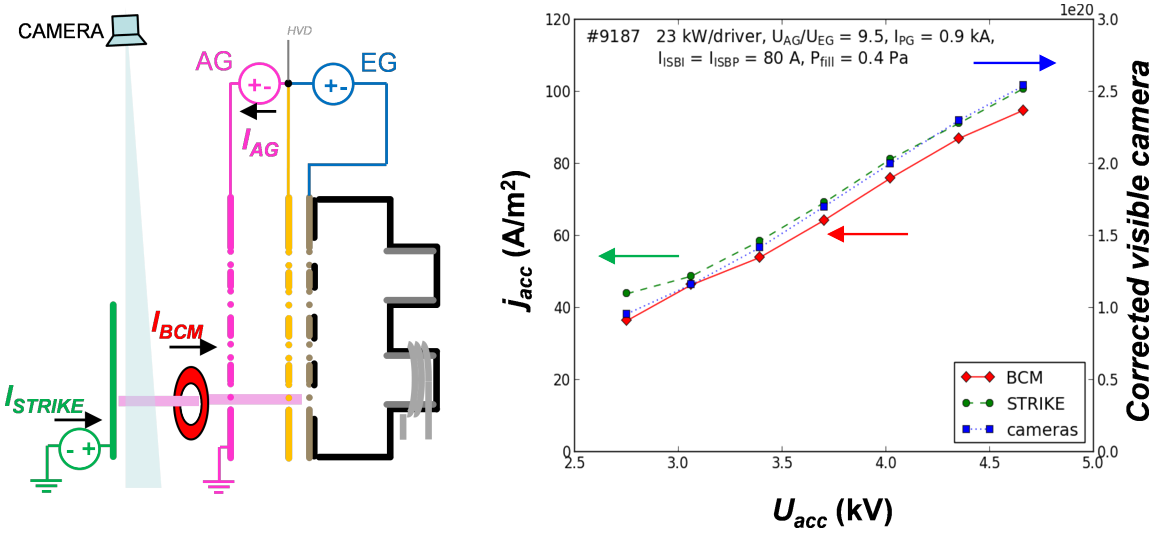

Figure 1. On the left, sketch of beam diagnostics, with the beamlet propagating from right to left from the ion source, through the accelerator, towards the beam dump. On the right, comparison of beamlet current measured by various diagnostics. In the figure, STRIKE is the instrumented beam dump, AG is the acceleration grid, EG is the extraction grid, BCM is a single-beamlet current sensor.

3 Control of caesium evaporation and improvement of the emission nozzle

While operating SPIDER in short pulses, it was found that the characteristics of the caesium flux from the caesium delivery system between plasma discharges was of great importance and could affect the beam uniformity and the capability of the plasma to redistribute the caesium [4]. Caesium distribution was studied density during operation [15, 16], as well as after the end of the operations with visual inspections and analyses of the ion source walls [17, 18]. It was found that the oven nozzle evaporated the largest caesium amount onto the surfaces in the proximity of the nozzle, creating stains that were clearly visible once the source was opened. In addition, over-heating of the oven nozzle during the plasma discharge occurred (with temperatures rapidly increasing from 200°C to 350°C even in 15s-long pulses), involving a rather extended length of the oven duct. This might determine a transient condition: the oven's surface could act as a temporary reservoir of caesium, which is promptly desorbed during the plasma discharge because of the temperature increase, and accumulates again before the next plasma pulse. This situation is different from the equilibrium one for which the caesium evaporation rate can be estimated. Due to air and water leaks, thick solid composites were found inside the oven reservoir and the estimation of the caesium consumption (by measuring the weight of the reservoid) to confirm the flow measured by the surface ionization detector was not possible. The caesium density measured by the laser absorption spectroscopy between plasma pulses, and the ceasium amount measured at the stains found at the extraction grid surfaces [17], were found to be in good agreement with the results of simulations (figure 2(a)) of caesium evaporation in vacuum [19].

2023 JINST 18 C09001

From the aforementioned experimental results, it was decided to improve the nozzle design with two purposes. Firstly, and most importantly, to minimize the evaporation flux onto the surrounding surfaces, to avoid such large concentrations of caesium (bottom half of figure 2(b)). Secondly, to attempt tailoring of the design of each of the three nozzles, aiming for a more uniform caesium flux towards the plasma grid and bias plate. Numerical models for the simulation of the caesium evaporation [20] and the characterization of the nozzle geometry [21] were developed in the past: the calculated caesium sticking on the plasma grid in the present configuration is shown in figure 2(a). Finally, it is proposed to minimize the heat load due to the interaction with the plasma by introducing permanent magnets above and below the nozzle; by calculating the leak width at the walls in correspondence of the magnets, the field line corresponding to the plasma edge can be derived. In the top half of figure 2(b), the red line indicates the plasma exclusion zone, obtained by following the field line intersecting the wall at the edge of the leak width (solid red line in front of the magnet). The latter results from the Hershkowitz approximation [22] for floating condition, which is only an indicative estimation, so that a large margin was taken with respect to the axial extent of the nozzle. The alternative solution of operating the oven at higher temperatures, so that transients during plasma on would have a minor impact, is not compatible with the present design [23]; oven operation during long pulses will have to be assessed in the future.

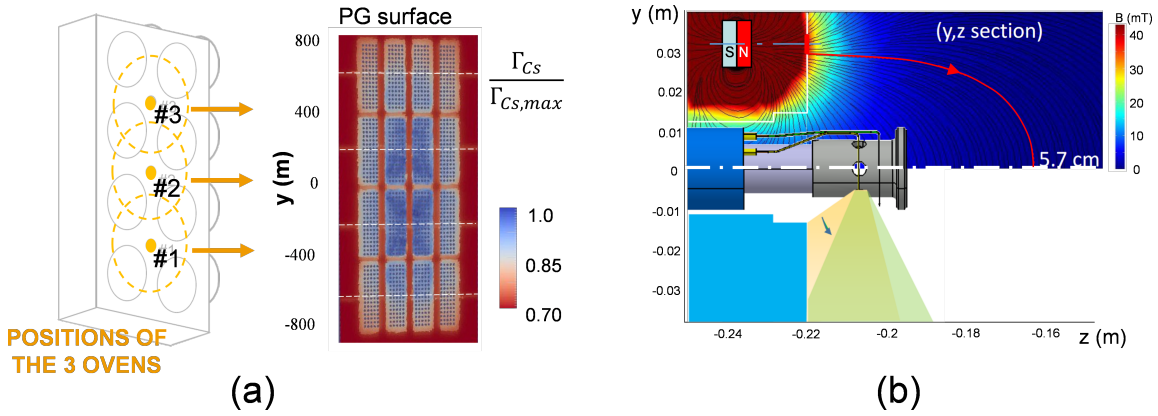

Figure 2. (a) Calculated caesium flux on PG, the shadowing effect of the bias plate is also visible; (b) calculated magnetic field strength and field lines; at the bottom, target emission cone for the nozzle optimization.

4 Vertical and horizontal homogeneity among RF drivers

Depending on the source parameters (i.e. pressure, filter field, RF power and bias voltages), the properties of the plasma inside the drivers – either measured by movable probes in the dedicated campaign [24] or by optical emission spectroscopy [25] – were found to be different from one driver to another [26]. A vertical non-homogeneity can be partially explained by plasma drifts downstream in the expansion region, which constitute the boundary condition of the drivers' plasmas. The power transmitted from the RF generators along the transmission lines, measured with directional couplers, was set to be equal, but it was not possible to confirm that the actual power coupled to the plasma was the same in the different drivers: on the contrary, the presence of mutual coupling among the four RF circuits onboard the source might add constructively or destructively to the self-induced

2023 JINST 18 C09001

flux of each circuit. The left/right non-homogeneity found experimentally is instead not easy to explain (see for instance the RF power scan in figure 3(b)), as the two coils are connected in series in the RF circuit; the left/right asymmetry was also found to depend, unexpectedly, on the filter field (as it uses field lines on the horizontal plane, it should only contribute to asymmetries on the vertical direction) and bias voltages. As the filter field is produced by current flowing in the plasma grid and on the return busbars, horizontal non-uniformity could be possible in case of unbalanced currents among the three return busbars: however, the absence of horizontal non uniformities of the PG current contribution was soon verified experimentally [27] (while about 10% variation of B strength along the vertical direction was confirmed). However, it was found that the configuration of permanent magnets installed on the lateral walls would produce a transverse field that is either summed or subtracted from the filter field produced by the currents, thus representing a possible cause for left/right asymmetry in the expansion of the plasma from the drivers. Finally, as extensively discussed in [12], the plasma at the extraction region and the accelerated single-beamlets exhibited non uniformities on the scale of the whole source but also within each group of beamlets.

The replacement of the four RF generators based on self-oscillators with solid-state RF generators [28–30] is expected to provide a large improvement, as the latter ones do not rely on internal resonance to set the frequency. In principle, this will avoid frequency instabilities (i.e. frequency flips), as well as allow direct control of the frequency to reach the best matching. An optimized layout of the RF circuit (matching network) next to the drivers was also designed [31], to minimise the mutual inductance (see figure 3(a)). This should improve the homogeneity of the power coupled to the plasma independently from the relative positions of the drivers. It is also expected that the solid-state generators will not be affected by cross-talk, especially when driven at the same frequency, and that there will be no modulation of RF power among the different pairs of drivers connected to each generator. The electrical circuit of the matching network on board the SPIDER source (shown in figure 3(c)) can be used to discuss the contribution of the parasitic capacitance between the RF coils and the source structure: such capacitance is in parallel to one of the two coils nominally connected in series, so that the current on the two coils might be different. The difference among the two RF coils in the pair has been estimated via Spice simulation to be between 2% and 4% in terms of current (i.e. RF power difference below 10%), considering values of parasitic capacity estimated experimentally. This effect alone cannot justify the differences seen experimentally, with a left/right ratio never approaching unity and in some cases at low power, such as the example in figure 3(b), reaching a value of two. Puzzlingly enough, the left/right asymmetry also depends on the filter field strength. The interaction between the field produced by the permanent magnets placed on the lateral walls and the filter field itself appears to be the cause: as shown in figure 4(a), the magnetization of the permanent magnets is sufficiently high to influence the plasma properties even far from the lateral walls, as the left/right differences on the B field strength almost reach the axis of the driver. Two-dimensional Particle-In-Cell simulations are being carried out to clarify the impact of such field configuration. Drifts and Hall currents in the plasma are not modelled if the plasma potential is solved only in the x,z plane, and therefore the influence of the magnetic field on the plasma expansion from the driver is not completely treated by two-dimensional simulations on the plane parallel to B; therefore, electron cooling through the filter is similar to the ideal 1D result, and plasma density may peak at the coordinate where B rapidly increases [32], and not inside the driver. Simulation results can anyway be discussed in comparative terms, focusing on the influence of permanent magnets at the lateral

2023 JINST 18 C09001

walls. The simulation is performed by fixing the background molecule and atom gas densities, and by applying a simplified heating mechanism through which electrons within the drivers are heated in a rather uniform manner; the scaling of ε_0 was necessary to allow the calculation on a 866×399 grid (see for instance the discussion in ref. [33]). Figure 4(b) shows a steady state map of the electron density, obtained with only filter field (produced by plasma grid currents and return busbars), indicating a symmetric condition. The non-symmetric density map of figure 4(c) was obtained by including also the permanent magnets at the lateral walls, clearly indicating that their effect extends to the lateral sides of the expansion region but also to the drivers. For this reason, a different design was developed for the cusp magnets embedded in the lateral walls, aiming at obtaining a good plasma confinement but a much reduced perturbation in the plasma center: smaller magnet size, but shorter thickness of the metallic structure between the magnets and the plasma (to have the same cusp strength at the plasma wall but lower field strength at greater distances), more columns of magnets (six columns instead of four, to close the field lines at a shorter distance inside the plasma) and finally alternate magnetization along the column (realizing a checkerboard configuration). It was also decided to deepen the understanding of the plasma-wall interaction at the lateral walls, a key region of the source because it is perpendicular to the filter field lines and therefore could easily become a great contribution to the plasma losses. Particle-in-cell simulations were carried out to calculate the loss fraction in a cusp field when the plasma potential is different than the floating potential [34] (in SPIDER, the plasma potential at the lateral walls is of the order of 30–50 V while the electron temperature is reduced between 5 and 1.5 eV), and also characterization of the deposits on the lateral wall surface was conducted [19], to clarify the extent of the plasma wall interaction. In order to allow a better experimental characterization of the discussed non uniformities, new diagnostics were designed to either characterize the homogeneity of the plasma properties among the drivers, or to measure the profiles of plasma properties in front of the extraction apertures [35, 36], integrating with the set of already existing diagnostics [37].

In the original design of the filter field return bus-bars, a strong transverse filter field permeated the driver region, and when the filter field strength was increased, the plasma progressively turned off [38]. The problem was solved by modifying the geometry and number of return conductors, so

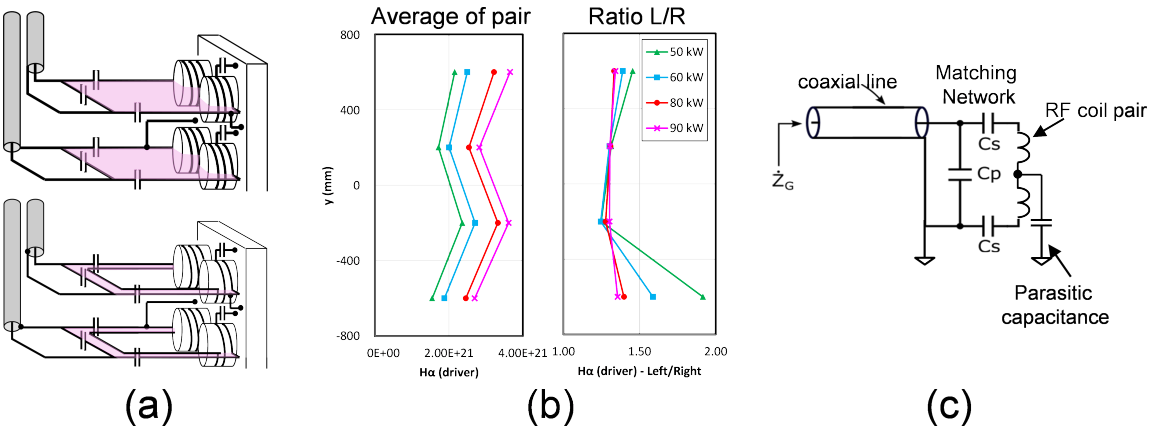

Figure 3. (a) reduction of the mutual inductance among RF circuit on-board SPIDER (b) measured Balmer α emission along a line of sight close to the driver axes during a RF power scan, highlighting vertical profile and left/right non-homogeneity (c) sketch of the RF circuit on-board SPIDER, indicating the matching network and the presence of parasitic capacitances at the coils.

2023 JINST 18 C09001

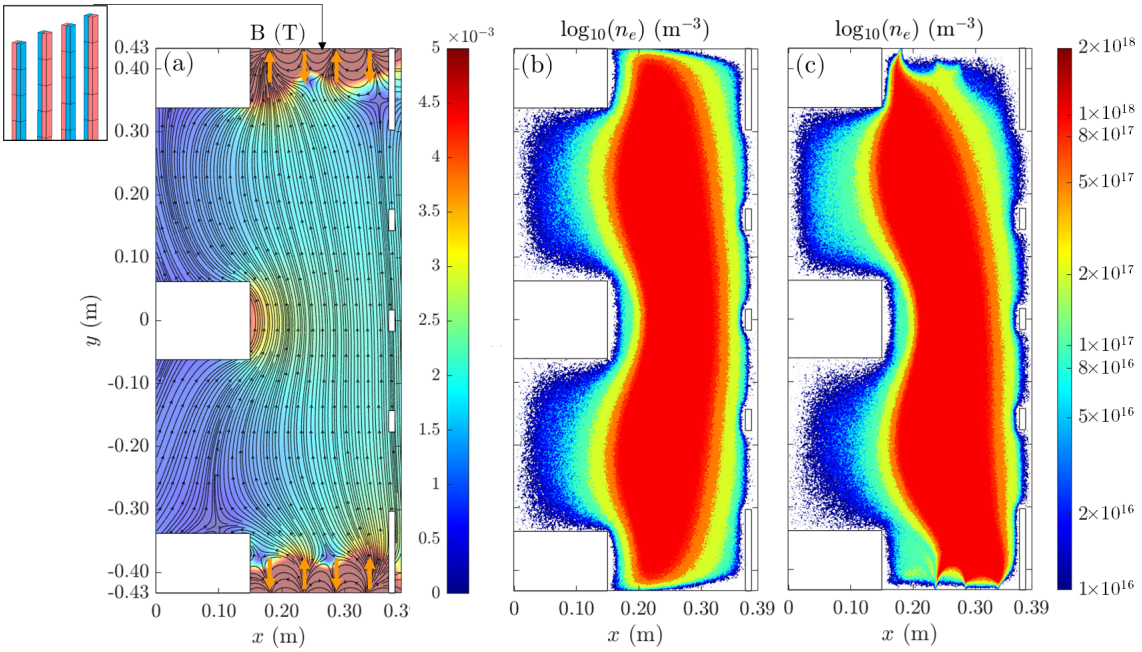

Figure 4. Horizontal section of SPIDER source: (a) magnetic field strength |B|, indicating also the magnetization of permanent magnets at lateral walls with respect to the direction of the filter field produced by currents (filter field directed from bottom to top); (b) electron density obtained in particle in cell simulation including only the filter field (c) same as b), but including permanent magnets at the lateral walls.

that the field intensity inside the drivers was strongly reduced, the presence of an X/null point for the field lines was avoided and the gradient of the magnetic field was reduced inside the driver volume. In inductively coupled plasma, it is commonly found that with external antennas the plasma can be pushed inward by Lorentz forces generated by RF-varying fields; however, early experimental evidence indicates that, in SPIDER, the presence of a magnetic field perpendicular to the driver axis can de-confine the plasma despite the presence of other confining effects. The reason for this effect can be discussed considering results of the bi-dimensional steady-state fluid model FSFS2D (Fluid Solver For SPIDER in 2D) [39], in the absence of a fully three-dimensional model. Recently, fluid equations in FSFS2D were weakly coupled to the RF-induced electric fields, considering in the fluid model the heating power due to induced currents in the plasma as an input for the electron energy equation, and in the electromagnetic model the plasma conductivity taken from the solution of the complex azimuthal induced electric field in cylindrical symmetry [40]. As shown in figure 5(a), when the plane perpendicular to the filter field is considered in a Cartesian geometry, the filter field is beneficial for confinement as the plasma transport perpendicular to B is impeded. However on the plane parallel to the filter field, as shown in figure 5(b), the presence of the filter field along y causes the very large electron diffusion parallel to B, and electrons can be lost to the driver edges (i.e. on the Faraday shield), thus providing a possible explanation for experimental behavior. It must be stated that simulating the plasma coupling on the plane perpendicular to the filter field provides a result which is, with respect to the experimental measurements obtained with movable probes inside the driver [24], quite the opposite: the few radial positions that were sampled experimentally generally showed a lower T_e next to the Faraday shield than at the center.

2023 JINST 18 C09001

5 Effect of magnetic fields on the plasma inside drivers

In the original design of the filter field return bus-bars, a strong transverse filter field permeated the driver region, and when the filter field strength was increased, the plasma progressively turned off [38]. The problem was solved by modifying the geometry and number of return conductors, so that the field intensity inside the drivers was strongly reduced, the presence of an X/null point for the field lines was avoided and the gradient of the magnetic field was reduced inside the driver volume. In inductively coupled plasma, it is commonly found that with external antennas the plasma can be pushed inward by Lorentz forces generated by RF-varying fields; however, early experimental evidence indicates that, in SPIDER, the presence of a magnetic field perpendicular to the driver axis can de-confine the plasma despite the presence of other confining effects. The reason for this effect can be discussed considering results of the bi-dimensional steady-state fluid model FSFS2D (Fluid Solver For SPIDER in 2D) [39], in the absence of a fully three-dimensional model. Recently, fluid equations in FSFS2D were weakly coupled to the RF-induced electric fields, considering in the fluid model the heating power due to induced currents in the plasma as an input for the electron energy equation, and in the electromagnetic model the plasma conductivity taken from the solution of the complex azimuthal induced electric field in cylindrical symmetry [40]. As shown in figure 5(a), when the plane perpendicular to the filter field is considered in a Cartesian geometry, the filter field is beneficial for confinement as the plasma transport perpendicular to B is impeded. However on the plane parallel to the filter field, as shown in figure 5(b), the presence of the filter field along y causes the very large electron diffusion parallel to B, and electrons can be lost to the driver edges (i.e. on the Faraday shield), thus providing a possible explanation for experimental behavior. It must be stated that simulating the plasma coupling on the plane perpendicular to the filter field provides a result which is, with respect to the experimental measurements obtained with movable probes inside the driver [24], quite the opposite, for the few radial positions that were sampled experimentally, that generally showed a lower T_e next to the Faraday shield than at the center.

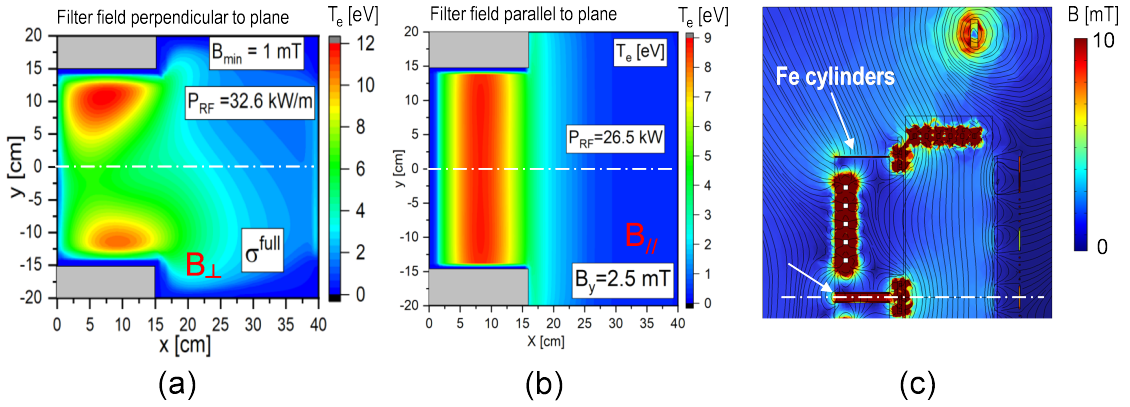

Figure 5. Comparison between electron temperature calculated by a fluid simulation with inductive coupling with FSFS2D code, on a vertical section (a) and on the horizontal section (b) for a single driver; (c) horizontal section view of magnetic field strength when a ferromagnetic cylinder is applied outside the RF antenna and electromagnetic screen around the RF driver.

2023 JINST 18 C09001

The presence of static magnetic fields inside the driver volume could be reduced with ferromagnetic material surrounding the driver volume, installed outside the electromagnetic screen (made of copper) which is already present around the RF coils. Such modification to the source design would provide, for a 4 mm thick ferromagnetic layer, a reduction inside the drivers to less than $\frac{1}{2}$ of the original value [27]; with this design solution, the filter field leaking in the driver would be only about 30% of the value in the expansion region (it is about 65% without ferromagnetic cylinders). Alternatively, if cusp magnets were installed around the cylindrical surface of the driver, they could counteract the transverse electron diffusion along the filter field lines, reducing the plasma loss at the walls as long as their field strength at the plasma boundary was higher than the filter field.

6 Single-beamlet optics

The best divergence measured in SPIDER at ~40 keV beam energy, at low RF power (23 kW/driver) and low filling pressure (between 0.3 and 0.35 Pa) was of the order of 12 mrad, coherently measured by all beam diagnostics. In addition, the Allison emittance scanner highlighted the presence of a broad component even along the direction perpendicular to the magnetic deflection along the accelerator, and even at low RF power. These values of divergence are rather high in comparison to multicusp filament-arc sources, which commonly achieve lower divergence for similar accelerator design at similar beam energies (see for instance [41]). In a sense, increasing the amount of negative ions available for extraction improves the divergence, as it allows operating at perveance match at larger beam energies, as required; however, we shall focus on the improvement of the divergence at perveance match for any extraction regime. Different possible approaches could be tried for improving divergence, starting from (*i*) the reduction of the energy of H^- precursors, to minimize their initial velocity when emitted at the converter surface, and from (*ii*) the increase of the positive ion density, while diminishing their temperature [42, 43], so that Coulomb collisions would help in reducing the negative ion temperature and direct them towards the extraction apertures.

Conversion from positive ions into negative ions at the plasma grid surface is, quantitatively speaking, a minor contribution to the negative ion generation at the caesiated surfaces, but a tail of fast negative ions can be produced if positive ions gain energy in the potential profile from the driver to the extraction region measured in SPIDER [24]. Fast atoms reaching the plasma grid can be generated by neutralization of ions accelerated by the potential profile towards the plasma grid, but also by plasma ion neutralization in the reflection at the rear walls of the ion source, which — taking as a reference the measurements of plasma parameters at the rear wall of the expansion chamber [44] — could be a rather significant contribution causing a high-energy tail of hot atoms up to 10–15 eV, with the sheath voltage being between 35 and 50 V at the rear walls. Numerical studies are being carried out to better quantify both volume processes and surface phenomena. A reduction of the ion flux on the rear walls of the source is possible by introducing cusp magnets [27]; this would in addition increase the plasma density by a non-negligible amount, given the large area of the rear source wall and the relatively high plasma density measured in its proximity. A decrease of the fast atom energy can be achieved by reducing the plasma potential and its gradients, which is also one of the main energy sources for positive ions. The integration of permanent magnets in the rear source walls influences the plasma role in the caesium recycling, as it reduces the extension of the plasma-wall interaction, although the major contribution in the removal of caesium from those

2023 JINST 18 C09001

surfaces is given by high energy backstreaming positive ions. This design change should also help in long pulse operation, allowing slower caesium release during beam acceleration.

Conversely, the reduction of the plasma potential inside the driver might require a reduction of the effective electron temperature; this is commonly achieved in multicusp sources for negative ions by increasing their confinement time, i.e. by having confinement magnets. The gradient of plasma potential tends to accelerate the negative ions backwards in the plasma, thus reducing their extraction probability; compensation by PG bias cannot act with the same effectiveness everywhere, due to the different plasma potential over the height of the source. A reduction of the plasma potential would additionally diminish, in part, the driving forces for vertical drifts (note that the diamagnetic drift caused by the electron pressure gradient cannot be removed, as it is also related to the electron cooling, a mandatory feature of negative ion sources). In addition to non-uniformities over the large extraction surface and therefore on the beam, vertical drifts may influence the single beamlet optics inducting deformation to the meniscus due to uneven fluxes at its surface (ref. [41] and references therein). To this purpose, it was proposed to install permanent magnets also around the drivers in addition to those around the expansion chamber [45]. Preliminary numerical simulations [46] showed a positive impact. However, due to space constraints, the technical implementation of this solution might have an impact on the coupling efficiency of the RF coils, and its effectiveness in reducing the electron and plasma potential shall be demonstrated experimentally before the integration in the SPIDER design.

In addition, plasma potential oscillations could also contribute to high-frequency modulation of the beam perveance; those oscillations in inductively coupled plasmas can be caused either by capacitive coupling to the coil, minimized if a Faraday shield is installed, or by the development of a RF polarization field along the radial direction. The effectiveness of retarding field energy analysers (RFEA) in measuring the overall time-averaged ion energy distribution (IED) at the plasma grid was demonstrated in SPIDER [24], also helping in studying the presence of plasma potential fluctuations; a wide ion energy distribution, markedly reducing in width when increasing the discharge pressure, was measured. For this reason, a RFEA to be permanently installed on the bias plate of SPIDER was designed [35], in such a way to continue the study and quantify the influence of source parameters on the IED and on the beamlet optics.

7 Expected conditions with improved pumping system

As mentioned, the vessel pressure influenced the discharge probability when operating the

RF drivers with multiple generators. The new pumping system was designed on the basis of Non Evaporable Getter technology [47], as recently developed [48]. The large pump, composed of many independent cartridges, will be installed behind the ion source, and requires the integration of thermal shields to protect in-vacuum components during high-temperature regeneration of the pump.

Due to the presence of the thermal shield, the effective pumping speed is reduced with respect to the installed one. Simulations were carried out with the three-dimensional numerical code based on view-factors Avocado [49]. The pumping speed of one cartridge of 0.87 m^3/s was applied, taken from experimental characterization at RT and 27 Pa m^3/kg of H_2 concentration (i.e. beginning of gas injection; at 625 Pa m^3/kg, it is about 25% lower). The results are shown in figure 6. Despite the difficulty in defining it, an effective pumping speed of 245 m^3/s was calculated considering

2023 JINST 18 C09001

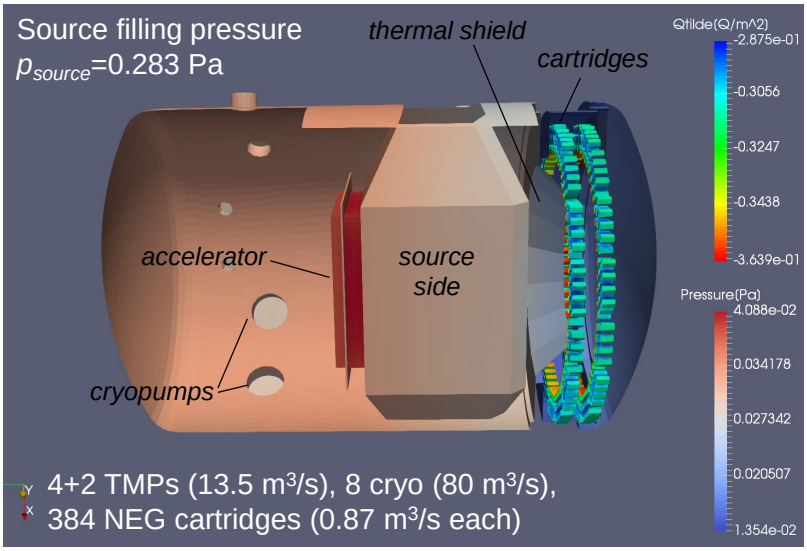

Figure 6. Pressure contours on the surface of in-vacuum components; on the surfaces of the getter cartridges, shown in the right hand side of the figure, the color contours indicate throughput per unit area Q/A.

the pressure on the rear side of the ion source, where it is needed. At 0.3 Pa filling pressure, the ratio source pressure over vessel pressure (on the pump side) is about 13, so that operating at higher pressures is also possible. From the experimental point of view, operating simultaneous of the pre-existing cryogenic system and the new non-evaporable getter system will require testing dedicated procedures for the coordination of the regeneration phases, to maximize the availability of the pumping system.

8 Conclusions

This paper reviewed selected experimental findings of the recent SPIDER operation, to discuss their relevance in view of the ITER heating neutral beams, and to provide an interpretation leading to design modifications of the plasma source and accelerator. SPIDER is presently in a shutdown, during which some of the proposed modifications are being implemented, and restarting is foreseen for the late 2023.

Acknowledgments

This work has been carried out within the framework of the ITER- RFX Neutral Beam Testing Facility (NBTF) Agreement and has received funding from the ITER Organization. The views and opinions expressed herein do not necessarily reflect those of the ITER Organization. This work has also been carried out within the framework of the EUROfusion Consortium, funded by the European Union via the Euratom Research and Training Programme (Grant Agreement No. 101052200 — EUROfusion). Views and opinions expressed are however those of the author(s) only and do not necessarily reflect those of the European Union or the European Commission. Neither the European Union nor the European Commission can be held responsible for them.

2023 JINST 18 C09001

References

[1] V. Toigo et al., *On the road to ITER NBIs: SPIDER improvement after first operation and MITICA construction progress*, *Fusion Eng. Des.* **168** (2021) 112622.

[2] B. Heinemann et al., *Towards large and powerful radio frequency driven negative ion sources for fusion*, *New J. Phys.* **19** (2017) 015001.

[3] G. Serianni et al., *SPIDER in the roadmap of the ITER neutral beams*, *Fusion Eng. Des.* **146** (2019) 2539.

[4] E. Sartori et al., *First operations with caesium of the negative ion source SPIDER*, *Nucl. Fusion* **62** (2022) 086022.

[5] M. Pavei et al., *SPIDER plasma grid masking for reducing gas conductance and pressure in the vacuum vessel*, *Fusion Eng. Des.* **161** (2020) 112036.

[6] A. Pimazzoni et al., *Co-extracted electrons and beam inhomogeneity in the large negative ion source SPIDER*, *Fusion Eng. Des.* **168** (2021) 112440.

[7] A. Shepherd et al., *Initial Results From the SPIDER Beamlet Current Diagnostic*, *IEEE Trans. Plasma Sci.* **50** (2022) 3906.

[8] A. Shepherd, T. Patton, B. Pouradier Duteil, A. Pimazzoni, A.R. Garola and E. Sartori, *Beam homogeneity of caesium seeded SPIDER using a direct beamlet current measurement*, *Fusion Eng. Des.* **192** (2023) 113599.

[9] M. Ugoletti et al., *SPIDER Beam Homogeneity Characterization Through Visible Cameras*, *IEEE Trans. Plasma Sci.* **50** (2022) 3913.

[10] A. Shepherd et al., *Direct current measurements of the SPIDER beam: a comparison to existing beam diagnostics*, in the proceedings of the 8^{th} *International Symposium on Negative Ions, Beams and Sources*, Orto Botanico, Padova, Italy, 2–7 October 2022, submitted to *JINST* [arXiv:2305.18001].

[11] G. Serianni et al., *SPIDER, the Negative Ion Source Prototype for ITER: Overview of Operations and Cesium Injection*, *IEEE Trans. Plasma Sci.* **51** (2023) 927.

[12] G. Serianni et al., *Spatially resolved diagnostics for optimization of large ion beam sources*, *Rev. Sci. Instrum.* **93** (2022) 081101.

[13] E. Sartori, V. Candeloro, M. Fadone, A. Pimazzoni and G. Serianni, *Influence of plasma grid-masking on the results of early SPIDER operation*, *Fusion Eng. Des.* **194** (2023) 113730.

[14] C. Poggi et al., *First tests and commissioning of the emittance scanner for SPIDER*, *Fusion Eng. Des.* **168** (2021) 112659.

[15] M. Barbisan et al., *Characterization of cesium and H-/D- density in the negative ion source SPIDER*, *Fusion Eng. Des.* **194** (2023) 113923 [arXiv:2211.04901].

[16] B. Pouradier Duteil et al., *Development of a Collisional Radiative Model for Hydrogen-Cesium Plasmas and Its Application to SPIDER*, *IEEE Trans. Plasma Sci.* **50** (2022) 3995.

[17] M. Pavei et al., *Status of SPIDER beam source after the first 3.5 years of operation*, *Fusion Eng. Des.* **192** (2023) 113831.

[18] V. Candela et al., *Investigations on Caesium Dispersion and Molybdenum Coating on SPIDER Components*, *Materials* **16** (2022) 206.

2023 JINST 18 C09001

[19] M. Fadone et al., *Summary of caesium evaporation and deposition during SPIDER first campaign*, in the proceedings of the 8^{th} *International Symposium on Negative Ions, Beams and Sources*, Orto Botanico, Padova, Italy, 2–7 October 2022, submitted to *JINST*.

[20] M. Fadone et al., *Interpreting the dynamic equilibrium during evaporation in a cesium environment*, *Rev. Sci. Instrum.* **91** (2020) 013332.

[21] E. Sartori, *Simulation-Based Quantification of Alkali-Metal Evaporation Rate and Systematic Errors From Current-Voltage Characteristics of Langmuir-Taylor Detectors*, *IEEE Trans. Instrum. Meas.* **69** (2020) 4975.

[22] M. Liebermann, *A. Lichtenberg, Principles of plasma discharges and materials processing*, Wiley & Sons (2005).

[23] M.D. Muri et al., *SPIDER cs ovens functional tests*, *Fusion Eng. Des.* **167** (2021) 112331.

[24] E. Sartori et al., *Development of a set of movable electrostatic probes to characterize the plasma in the ITER neutral beam negative-ion source prototype*, *Fusion Eng. Des.* **169** (2021) 112424.

[25] M. Ugoletti et al., *Study of the relationship between the source complexity and the beam divergence and homogeneity in SPIDER*, in the proceedings of the 8^{th} *International Symposium on Negative Ions, Beams and Sources*, Orto Botanico, Padova, Italy, 2–7 October 2022, submitted to *JINST*.

[26] P. Jain et al., *Use of electrical measurements for non-invasive estimation of plasma electron density in the inductively coupled SPIDER ion source*, accepted in *Plasma Phys. Control. Fusion* (2023).

[27] N. Marconato, E. Sartori and G. Serianni, *Numerical and Experimental Assessment of the New Magnetic Field Configuration in SPIDER*, *IEEE Trans. Plasma Sci.* **50** (2022) 3884.

[28] A. Maistrello et al., *Overview on electrical issues faced during the SPIDER experimental campaigns*, *Fusion Eng. Des.* **190** (2023) 113510 [arXiv:2304.02294].

[29] D. Marcuzzi et al., *Lessons learned after three years of SPIDER operation and the first MITICA integrated tests*, *Fusion Eng. Des.* **191** (2023) 113590 [arXiv:2304.01692].

[30] R. Casagrande, *Guidelines for the integration of RF solid state generators for the high power ion sources of NBTF experiments and ITER HNB*, presented in the *32nd Symposium on Fusion Technology — SOFT 2022*, Dubrovnik, Croatia, 18–23 September 2022, submitted to *Fusion Eng. Des.*

[31] M. Recchia et al., *Improvement in the electrical design of the SPIDER beam source Layout RF a bordo sorgente*, presented in the *32nd Symposium on Fusion Technology — SOFT 2022*, Dubrovnik, Croatia, 18–23 September 2022, submitted to *Fusion Eng. Des.*

[32] J.P. Boeuf, B. Chaudhury and L. Garrigues, *Physics of a magnetic filter for negative ion sources. I. Collisional transport across the filter in an ideal, 1D filter*, *Phys. Plasmas* **19** (2012) 113509.

[33] V. Candeloro, E. Sartori and G. Serianni, *Electron Scraping and Electron Temperature Reduction by Bias Electrode at the Extraction Region of a Large Negative Ion Source*, *IEEE Trans. Plasma Sci.* **50** (2022) 3983.

[34] V. Candeloro, E. Sartori and G. Serianni, *Influence of plasma parameters on the effectiveness of multi-cusp magnetic field confinement in negative ion sources*, 2023 *JINST* **18** C06028.

[35] B. Segalini et al., *Study and development of diagnostic systems to characterise the extraction region in SPIDER*, in the proceedings of the 8^{th} *International Symposium on Negative Ions, Beams and Sources*, Orto Botanico, Padova, Italy, 2–7 October 2022, submitted to *JINST*.

[36] R. Pasqualotto et al., *Improvement of SPIDER diagnostic systems*, *Fusion Eng. Des.* **194** (2023) 113889.

2023 JINST 18 C09001

[37] C. Poggi et al., *Highly electronegative plasma conditions in the SPIDER negative ion source*, in the proceedings of the 8^{th} *International Symposium on Negative Ions, Beams and Sources*, Orto Botanico, Padova, Italy, 2–7 October 2022, submitted to *JINST*.

[38] N. Marconato et al., *An optimized and flexible configuration for the magnetic filter in the SPIDER experiment*, *Fusion Eng. Des.* **166** (2021) 112281.

[39] R. Zagórski, E. Sartori and G. Serianni, *2-D Fluid Model for Discharge Analysis of the RF-Driven Prototype Ion Source for ITER NBI (SPIDER)*, *IEEE Trans. Plasma Sci.* **50** (2022) 4002.

[40] R. Zagórski, D. López-Bruna, E. Sartori and G. Serianni, *2d simulations of inductive RF heating in the drivers of the SPIDER device*, *Fusion Eng. Des.* **188** (2023) 113427.

[41] P. Veltri et al., *Ion beam transport: modelling and experimental measurements on a large negative ion source in view of the ITER heating neutral beam*, *Nucl. Fusion* **57** (2017) 016025.

[42] A. Pimazzoni, E. Sartori, G. Serianni and P. Veltri, *Influence of positive ions on the beamlet optics for negative-ion neutral beam injectors*, *Nucl. Fusion* **63** (2023) 076031.

[43] A. Pimazzoni et al., *Key parameters for the ion velocity distribution at the plasma meniscus of a caesiated negative ion source*, in the proceedings of the 8^{th} *International Symposium on Negative Ions, Beams and Sources*, Orto Botanico, Padova, Italy, 2–7 October 2022, submitted to *JINST*.

[44] V. Candeloro et al., *Development of a Triple Langmuir Probe for Plasma Characterization in SPIDER*, *IEEE Trans. Plasma Sci.* **50** (2022) 3871.

[45] N. Marconato, G. Berton, V. Candeloro, E. Sartori, B. Segalini and G. Serianni, *Integration of new sets of magnets for improved plasma confinement in the SPIDER experiment*, *Fusion Eng. Des.* **193** (2023) 113805.

[46] R. Zagórski et al., *Influence of different magnetic configuration on plasma parameters in SPIDER device*, in the proceedings of the 8^{th} *International Symposium on Negative Ions, Beams and Sources*, Orto Botanico, Padova, Italy, 2–7 October 2022, submitted to *JINST*.

[47] E. Sartori et al., *Design of a large nonevaporable getter pump for the full size ITER beam source prototype*, *J. Vac. Sci. Tech. B* **41** (2023) 034202.

[48] E. Sartori et al., *Development of non evaporable getter pumps for large hydrogen throughput and capacity in high vacuum regimes*, *Vacuum* **214** (2023) 112198.

[49] E. Sartori and P. Veltri, *AVOCADO: A numerical code to calculate gas pressure distribution*, *Vacuum* **90** (2013) 80.

2023 JINST 18 C09001